# A faster numerical scheme for a coupled system modeling soil erosion and sediment transport

Minh-Hoang Le, Stéphane Cordier, Carine Lucas, Olivier Cerdan

# A faster numerical scheme for a coupled system modelling soil erosion and sediment transport

M.-H. Le*, S. Cordier†, C. Lucas‡and O. Cerdan§

**Abstract**

Overland flow and soil erosion play an essential role in water quality and soil degradation. Such processes, involving the interactions between water flow and the bed sediment, are classically described by a well-established system coupling the shallow water equations and the Hairsine-Rose model. Numerical approximation of this coupled system requires advanced methods to preserve some important physical and mathematical properties; in particular the steady states and the positivity of both water depth and sediment concentration. Recently, finite volume schemes based on Roe's solver have been proposed by *Heng et al.* (2009) and *Kim et al.* (2013) for one and two-dimensional problems. In their approach, an additional and artificial restriction on the time step is required to guarantee the positivity of sediment concentration. This artificial condition can lead the computation to be costly when dealing with very shallow flow and wet/dry fronts. The main result of this paper is to propose a new and faster scheme for which only the CFL condition of the shallow water equations is sufficient to preserve the positivity of sediment concentration. In addition, the numerical procedure of the erosion part can be used with any well-balanced and positivity preserving scheme of the shallow water equations. The proposed method is tested on classical benchmarks and also on a realistic configuration.

## 1 Introduction

Soil erosion by water is a complex phenomenon affected by many factors such as climate, topography, soil characteristics, vegetation and anthropogenic activities (e.g. cultivation practices) (*Cerdan et al.*, 2010). Soil erosion and sediment transport can have adverse effects on the stormwater quality (*Quinton et al.*, 2010). Erosion processes due to rainfall and overland flow can be described in three stages: detachment, transport and deposition of soil particles. Advanced mathematical models focus on the simulating of hydrodynamic processes coupling with sediment transport and morphological evolution. These approaches, sometimes called physically based models, rely on the conservation of mass and energy principles. Several review papers on existing models can be found in literature where the hydrodynamic erosion processes were described at plot or catchment scales (see e.g. *Merritt et al.*, 2003; *Aksoy and Kavvas*, 2005). In general, water flow can be described by the well-known Navier-Stokes equation but in context of shallow flow, a simplified model called the shallow water (SW)

*Univ. Orléans, CNRS, MAPMO, UMR 7349, Fédération Denis Poisson, F-45067, Orléans, France and BRGM, Risks Department, 3 rue Claude Guillemin, 45060 Orléans, France, (Minh.Hoang.Le@math.cnrs.fr).

†Univ. Orléans, CNRS, MAPMO, UMR 7349, Fédération Denis Poisson, F-45067, Orléans, France, (Stéphane.Cordier@univ-orleans.fr).

‡Univ. Orléans, CNRS, MAPMO, UMR 7349, Fédération Denis Poisson, F-45067, Orléans, France, (Carine.Lucas@univ-orleans.fr).

§BRGM, Risks Department, 3 rue Claude Guillemin, 45060 Orléans, France, (O.Cerdan@brgm.fr).

equations are commonly used (*Hervouet*, 2007). On the erosion part, the sediment transport by water can be described by equations of sediment mass conservation with source terms.

The source terms in the sediment transport equations express detachment and deposition processes. Its formulas can be classified into two categories. The first one treats erosion processes with only one (representative) sediment size. Related works can be found, for example, in the publications of *Nord and Esteves* (2005); *Murillo et al.* (2008); *Cao et al.* (2004); *Simpson and Castelltort* (2006); *Li and Duffy* (2011). Moreover, most of these models adopt the transport capacity concept to distinguish the erosion and deposition situations. Several related limitations have been noted (*Sander et al.*, 2007). It is well known that soil erodibility depends on the particle size distribution and the deposition is a size-selective process (*Farenhorst and Bryan*, 1995). The need to use a more advanced model, to quantify the rate of detachment and/or deposition, has been suggested (see e.g. *Nord and Esteves*, 2005; *Murillo et al.*, 2008). The second type approach takes into account the particle's size distribution and their impacts on the process of erosion and sediment transport. The approach proposed by *Hairsine and Rose* (1991, 1992), called the HR model hereafter, is such a model. In addition, this multi-size class model considers the detachment-entrainment of the original soil, the redetachment-reentrainment of deposited sediments and the sedimentation as concurrent processes. An important feature of this model is the proposition of continuous deposition that creates a sediment layer protection the original soil from erosive forces (*Govers et al.*, 2007). This model has been investigated and applied with some successes to various scenarios of soil erosion both at plot and catchment scales (see e.g. *Fiener et al.*, 2008; *Van Oost et al.*, 2004; *Heng et al.*, 2011; *Kim et al.*, 2013).

With the SW equations, a well-known difficulty of numerical solvers is to preserve the steady states, to deal with large bottom slopes and wet/dry transitions. Such a solver is called a well-balanced scheme whose construction is of interest to many researchers. A large variety of advanced numerical solvers are able to produce accurate results (see e.g. *Gallouët et al.*, 2003; *Audusse and Bristeau*, 2005; *Castro et al.*, 2006; *Liang and Marche*, 2009; *Bouchut and de Luna*, 2010; *Berthon and Foucher*, 2012; *Duran et al.*, 2013; *Hou et al.*, 2013, and the references given therein as a non exhaustive list). These papers have shown that the numerical discretization of the bathymetry needs to be related to that of the convective flux to avoid spurious oscillations appearing in the solution. On the modelling of erosion processes, we observe that the numerical method for the coupled system SW-HR has been relatively less studied except by *Heng et al.* (2009) and *Kim et al.* (2013). They used the Roe-type approximate Riemann schemes to solve one- and two-dimensional problems respectively.

The present work concerns the numerical simulation of soil erosion processes using the coupled system SW-HR. We are interested in applying the cited well-balanced schemes for the hydrodynamic part. An interesting feature of these methods is that the numerical fluxes guarantee the positivity of the water depth at every control volume throughout the computation. Based on this property, we propose and analyze a simple and robust numerical discretization for the sediment transport equation linking the erosion part with the hydrodynamic one. It will be shown that the resulting method is well-balanced and ensures the positivity of the water depth and the sediment concentration under the classical CFL (Courant-Friedrichs-Lewy) condition of the SW equations.

The outline of the paper is as follows: in section 2, we present the system of governing equations with the same notations as those in *Heng et al.* (2009) and *Kim et al.* (2013). In section 3, we describe our numerical scheme and analyze its main features. Next, we validate the proposed method in section 4 with several benchmarks selected from the literature. We justify the quality of the scheme in terms of performance by a two-dimensional test on a realistic configuration.

## 2 System coupling hydrodynamic, erosion and sediment transport

In this section, we recall the governing system of equations that has been studied by *Heng et al.* (2009) and *Kim et al.* (2013). This consists of a system coupling the two-dimensional SW equations with the HR model for $I$ classes of sediment, namely

$$\begin{cases} \partial_t h + \nabla \cdot (h\mathbf{u}) = R - I_r, \\ \partial_t (h\mathbf{u}) + \nabla \cdot (h\mathbf{u} \otimes \mathbf{u}) + \nabla \left( \dfrac{gh^2}{2} \right) = -gh(\nabla z_b + S_f), \\ \partial_t (c_i h) + \nabla \cdot (c_i h\mathbf{u}) = e_i + e_{ri} + r_i + r_{ri} - d_i, \\ \partial_t m_i = d_i - e_{ri} - r_{ri}, \\ (1-\phi)\rho_s \partial_t z_b = \displaystyle\sum_{i=1}^{I} (d_i - e_i - e_{ri} - r_i - r_{ri}), \end{cases} \tag{1}$$

(for $i = 1, \ldots, I$), where the $(2I + 4)$ unknowns of system are

- $h$ the water depth [L],
- $\mathbf{u} = (u, v)$ the horizontal velocity of the flow [L/T],
- $z_b$ the bed surface elevation [L],
- $c_i$ the sediment concentration of $i$-th class [M/L$^3$],
- $m_i$ their mass in the deposited layer [M/L$^2$].

Let us recall the source terms of the SW equations: the water source terms are $R$ and $I_r$ [L/T] representing the rainfall intensity and the infiltration rate respectively. For the friction slope $S_f$, two formulations are usually chosen in hydrological models: the Manning friction law $S_f = \mathrm{n}^2 \mathbf{u}|\mathbf{u}|/\mathrm{h}^{4/3}$ or the Darcy-Weisbach law $S_f = f\mathbf{u}|\mathbf{u}|/(8gh)$. Both the Manning friction coefficient n and the Darcy-Weisbach coefficient $f$ [−] are regarded as constants. Finally, $\phi$ [−] represents the porosity of eroded bed and $g$ [L/T$^2$] the gravity acceleration.

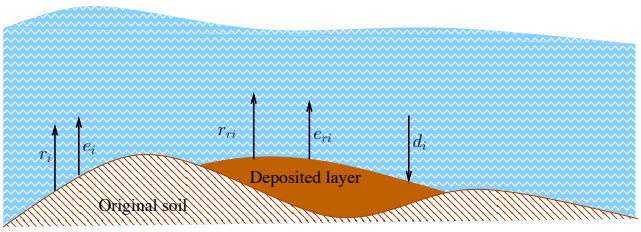


Figure 1: Processes interacting between the original soil, deposited layer and suspended sediments in overland flow.

The HR model describes the erosion processes of $I$ particle-size classes, as illustrated in Fig. 1. Note that this model considers the detached sediments as passive pollutants in the flow. In other words, the concentration of sediment is supposed to have no influence on the equations governing the water dynamics. This hypothesis is fulfilled, for example, when the concentration in volume of sediment is less than 10%. On the contrary, simulating a hyper-concentration of sediment requires sometimes a

strong coupling with the equations governing the water flow (see e.g. *Cao et al.*, 2002, 2004; *Simpson and Castelltort*, 2006; *Li and Duffy*, 2011).

For the $i$-th class, $v_{fi}$ [L/T] is the settling velocity, $e_i$ and $r_i$ [M/L$^2$/T] are the rates of rainsplash detachment and flow entrainment from the original soil respectively, $e_{ri}$ and $r_{ri}$ [M/L$^2$/T] are the rates of rainsplash re-detachment and flow re-entrainment from the deposited layer respectively and finally $d_i$ [M/L$^2$/T] is the deposition rate. These source terms are given by:

$$e_i = (1-H)p_i a R, \tag{2}$$

$$e_{ri} = H\frac{m_i}{m_T}a_d R, \tag{3}$$

$$r_i = (1-H)p_i\frac{F(\omega-\omega_{cr})}{J}, \tag{4}$$

$$r_{ri} = H\frac{m_i}{m_T}\frac{F(\omega-\omega_{cr})}{\frac{\rho_s-\rho_w}{\rho_s}gh}, \tag{5}$$

$$d_i = c_i v_{fi}, \tag{6}$$

where $a$ and $a_d$ [M/L$^3$] are the detachability coefficients of the original soil and the deposited layer respectively, $\rho_w$ and $\rho_s$ [M/L$^3$] the densities of water and sediment respectively, and $p_i$ [$-$] the fraction of $i$-th class in the original soil.

As soil erosion due to flow is a threshold process, the stream power $\omega = \rho_w gh|S_f||\mathbf{u}|$ must exceed the critical value $\omega_{cr}$ [M/T$^3$] to entrain soil particles. In such a situation, $F$ ($-$) is the effective fraction of excess stream power in entrainment and re-entrainment, and $J$ [ML$^2$/T$^2$/M] is the energy expended in entraining a unit mass of cohesive sediment. Once the deposited layer has been created, it protects the original soil and consequently reduces the rate of detachment and entrainment of the original soil. To characterise this effect, we define $H = \min\{1, m_T/m_T^*\}$ the fractional shielding of the original soil by the deposited layer, with $m_T = \sum_{i=1}^{I} m_i$ the accumulated mass per unit area of deposited layer and $m_T^*$ [M/L$^2$] the required mass of deposited layer to shield completely the original soil. The modelling of this process is a new and advanced point of the HR model compared to the others (*Govers et al.*, 2007).

Since the raindrop energy is reduced as it penetrates the surface water layer, the soil detachability coefficients $a$, $a_d$ and the critical mass $m_T^*$ are decreasing functions of the water depth $h$. *Proffitt et al.* (1991) proposed the following power law

$$\begin{pmatrix} a \\ a_d \end{pmatrix} = \begin{pmatrix} a_0 \\ a_{d0} \end{pmatrix} \times \begin{cases} 1 & \text{if } h \le h_0 \\ (h_0/h)^b & \text{if } h > h_0 \end{cases} \tag{7}$$

and *Heng et al.* (2011) complemented this relation by

$$m_T^* = m_{T0}^* \times \begin{cases} 1 & \text{if } h \le h_0 \\ (h_0/h)^b & \text{if } h > h_0 \end{cases}$$

where $a_0, a_{d0}$ and $m_{T0}^*$ are the related maximum values at the breakpoint depth $h_0$ which is about 0.33 times the mean drop diameter, and $b$ is an exponent depending on the type of soil. This equation was used in *Heng et al.* (2011) and *Kim et al.* (2013).

In the next section, we explain how to discretize equations (1)–(6), paying attention to preserve physical properties such as non-negativity of the water height and the sediment concentration.

## 3 Numerical method

Finite volume schemes are known to be robust for the numerical simulation of conservative systems since this method ensures their conservation by construction. The method for solving a multidimensional system is described in detail in *LeVeque* (2002) for example. Briefly for the two-dimensional problem (1) that we can rewrite in generic form

$$\partial_t \mathbf{w} + \nabla \cdot \mathbf{f}(\mathbf{w}) = \mathbf{s}(\mathbf{w}),$$

the basic principle of the method is to integrate the considered system over a *control volume* $\mathcal{C}$ of the mesh and use the divergence theorem to obtain

$$\int_{\mathcal{C}} \partial_t \mathbf{w} \; d\mathbf{x} + \int_{\Gamma} \mathbf{f} \cdot \vec{\mathbf{n}} \; d\Gamma = \int_{\mathcal{C}} \mathbf{s}(\mathbf{w}) \; d\mathbf{x},$$

where $\Gamma$ stands for the boundary of the control volume and $\vec{\mathbf{n}}$ its outward unit vector normal. The first term concerning the time derivative is always computed with a finite difference method while the right hand side expresses the total source applied on the control volume. A key aspect of any finite volume scheme consists of evaluating the flux $\mathbf{f} \cdot \vec{\mathbf{n}}$ over the interfaces of control volumes. From this principle, the extension of an existing one-dimensional numerical scheme to the two-dimensional case is straightforward, especially with the schemes based on the Riemann solvers (*Toro*, 2001) as used here. For the sake of simplicity, we only describe hereafter the numerical method for the one-dimensional system.

In the present work, we propose a numerical finite volume scheme, as in *Heng et al.* (2009); *Kim et al.* (2013), but the treatment of the equations is different. Two main characteristics of the proposed method are: (*i*) it makes the numerical coupling of erosion part becoming less dependent on the numerical solvers of hydrodynamic part; so that many recent and advanced schemes/computation codes on the SW equations can be used. (*ii*) it relaxes the additional restriction on the time step related to the HR equations. Only the CFL condition of the SW system is sufficient to guarantee the stabilization of the numerical solution.

Introducing the conservative variables

$$\mathbf{U} = \begin{pmatrix} h \\ hu \\ c_1 h \\ \vdots \\ c_I h \end{pmatrix}, \quad \mathbf{V} = \begin{pmatrix} m_1 \\ \vdots \\ m_I \\ z_b \end{pmatrix},$$

the one-dimensional system of governing equations becomes

$$\begin{cases} \partial_t \mathbf{U} + \partial_x F(\mathbf{U}) = S_0 + S_1, \\ \partial_t \mathbf{V} = S_2, \end{cases}$$

where the flux and the source terms are given by

$$F(\mathbf{U}) = \begin{pmatrix} hu \\ hu^2 + gh^2/2 \\ c_1 hu \\ \vdots \\ c_I hu \end{pmatrix}, \quad S_0 = \begin{pmatrix} 0 \\ -gh\partial_x z_b \\ 0 \\ \vdots \\ 0 \end{pmatrix},$$

$$S_1 = \begin{pmatrix} R - I_r \\ -ghS_f \\ e_1 + e_{r1} + r_1 + r_{r1} - d_1 \\ \vdots \\ e_I + e_{rI} + r_I + r_{rI} - d_I \end{pmatrix},$$

$$S_2 = \begin{pmatrix} d_1 - e_{r1} - r_{r1} \\ \vdots \\ d_I - e_{rI} - r_{rI} \\ \frac{\sum_{i=1}^{I}(d_i - e_i - e_{ri} - r_i - r_{ri})}{(1-\phi)\rho_s} \end{pmatrix}.$$

Note that the topographical source term $S_0$ contains the derivative $\partial_x z_b$ corresponding to the bottom slope while $S_1$ and $S_2$ are cell-centered terms related to water source terms, bed friction, erosion and deposition. For this reason, $S_0$ needs to be discretized together with the flux $F(\mathbf{U})$. On the contrary, $S_1$ and $S_2$ can be treated in a separate step by a system of ordinary differential equations (ODE), without adding numerical oscillations. In other words, we adopt a time-splitting strategy that first solves the following hyperbolic system with source term $S_0$ (called convective step)

$$\partial_t \mathbf{U} + \partial_x F(\mathbf{U}) = S_0,$$

and then correct the computed value by taking into account the source terms $S_1$ and $S_2$ via the system

$$\begin{cases} \partial_t \mathbf{U} = S_1, \\ \partial_t \mathbf{V} = S_2. \end{cases}$$

Note that a scheme which is second-order accurate in time can be reached by repeating these two steps with Heun's method, *i.e.* the second-order total variation diminishing (TVD) Runge-Kutta scheme. In the following it is sufficient to only consider a numerical scheme which is second order in space but first order in time.

### 3.1 Convective step

We notice that in the convective step, the $I$ transport equations of sediment concentrations have the same form. For the sake of compactness, the last $I$ equations are replaced by a generic one, using $c$ instead of $c_i$ to denote the concentration of the considered sediment-size class. Then, the compacted system is writen as

$$\partial_t h + \partial_x(hu) = 0, \tag{8}$$

$$\partial_t(hu) + \partial_x(hu^2 + gh^2/2) = -gh\partial_x z_b, \tag{9}$$

$$\partial_t(ch) + \partial_x(chu) = 0. \tag{10}$$

Starting from a given value $\mathbf{U}^n$, the variables obtained after this step are denoted with a bar: $\overline{h}, \overline{hu}, \overline{ch}$.

### 3.1.1 Numerical schemes for the shallow water equations

These schemes are aimed at solving the well-known SW equations (8)–(9). Since this system contains source terms, a numerical approximation must be made with more attention focussed on capturing exactly the steady states of the system, *i.e.* the exact functions $h, u$ satisfying

$$hu = \text{const. and } u^2/2 + g(h + z_b) = \text{const.} \tag{11}$$

These solvers are called *well-balanced methods* since the pioneering work of *Greenberg and LeRoux* (1996). Moreover, it is well-known that small water depths near wet-dry interfaces can lead to numerical instabilities. Numerical treatment of wet-dry fronts is thus a challenge when simulating shallow flow over nonuniform bathymetries (*Bouchut*, 2004).

The numerical discretization of the SW equations has been extensively studied. A large variety of proposed numerical solvers are able to produce accurate results. A non-exhaustive list of these methods can be found in (*Gallouët et al.*, 2003; *Audusse et al.*, 2004; *Audusse and Bristeau*, 2005; *Castro et al.*, 2006; *Liang and Marche*, 2009; *Bouchut and de Luna*, 2010; *Berthon and Foucher*, 2012; *Duran et al.*, 2013; *Hou et al.*, 2013). These finite volume schemes can be rewritten in the following generic conservative form

$$\overline{U}_j = U_j^n - \frac{\Delta t}{\Delta x}\left(F_{j+1/2L} - F_{j-1/2R}\right) \tag{12}$$

where the vector $\overline{U}_j$ stands for the updated state $(\overline{h}_j,\ \overline{h_j u_j})^t$ obtained from the given one $U_j^n$ on the current cell $j$; $\Delta x, \Delta t$ are the space and time steps respectively; $F_{j+1/2L,R} = (F_{L,R}^h,\ F_{L,R}^{hu})^t := F_{L,R}(U_j^n, U_{j+1}^n, \Delta z_{bj+1/2})$ are the left and right numerical fluxes in which $\Delta z_{bj+1/2} = z_{bj+1} - z_{bj}$. In the computation of $F_{j+1/2L,R}$, we can replace the given state $(U_j^n, U_{j+1}^n)$ by its high order approximation at the interface, e.g. using the MUSCL reconstruction (*van Leer*, 1979), to get the high order scheme.

The cited numerical schemes differ from each other in the construction of $F_{L,R}(U_j^n, U_{j+1}^n, \Delta z_{bj+1/2})$ which satisfy the following conditions (see *Bouchut*, 2004):

1. conservativity of the water depth, *i.e.*

$$F_L^h(U_j^n, U_{j+1}^n, \Delta z_{bj+1/2}) = F_R^h(U_j^n, U_{j+1}^n, \Delta z_{bj+1/2}) := F_{j+1/2}^h \tag{13}$$

2. consistency with the homogeneous system, *i.e.* $F^h(U, U, 0) = hu$, $F_L^{hu}(U, U, 0) = F_R^{hu}(U, U, 0) = hu^2 + gh^2/2$,

3. asymptotic conservativity/consistency with the source term, *i.e.* $F_{j+1/2R}^{hu} - F_{j+1/2L}^{hu} = -gh\Delta z_{bj+1/2} + o(\Delta z_{bj+1/2})$ when $U_j^n \to U_{j+1}^n$ and $\Delta z_{bj+1/2} \to 0$,

4. well-balancing, *i.e.* given the discrete steady states $(U_j^n, U_{j+1}^n, \Delta z_{bj+1/2})$ satisfying (11) as the numerical fluxes must satisfy $F_{j+1/2L} = F(U_j^n)$ and $F_{j+1/2R} = F(U_{j+1}^n)$ where $F(U) := (hu,\ hu^2 + gh^2/2)^t$ stands for the physical flux of the SW equations.

Defining $s_{L,R} = u \pm \sqrt{gh}$ the slowest and fastest wave speeds of the SW equations, a well-known restriction on the space and time steps, called the CFL condition, is required for the stability of numerical solution

$$\frac{\Delta t}{\Delta x}\max\{|s_L|, |s_R|\} \leq C \tag{14}$$

with $C = 1$ for the first order scheme, and $C = 0.5$ in the case of a second order scheme.

Note that from (12) and (13), the computation of the water depth reads

$$\overline{h}_j = h_j^n - \frac{\Delta t}{\Delta x}\left(F_{j+1/2}^h - F_{j-1/2}^h\right). \tag{15}$$

It should be shown that under the CFL condition (14), the fluxes $F_{j+1/2L,R}$ preserve the *positivity at interface* (*Bouchut*, 2004) of the water depth in the sense that

$$\begin{aligned} \overline{h}_{j+1/2L} &:= h_j^n - \frac{2\Delta t}{\Delta x}\left(F_{j+1/2}^h - h_j^n u_j^n\right) \geq 0, \\ \overline{h}_{j-1/2R} &:= h_j^n - \frac{2\Delta t}{\Delta x}\left(h_j^n u_j^n - F_{j-1/2}^h\right) \geq 0. \end{aligned} \tag{16}$$

Consequently, the positivity of the water depth at every control volume throughout the computation is automatically guaranteed since $\overline{h}_j = 0.5(\overline{h}_{j-1/2R} + \overline{h}_{j+1/2L})$. In section 3.1.2, we will exploit the property (16) to construct a simple and robust numerical scheme for the sediment transport problem.

In the present work, the scheme proposed by *Audusse et al.* (2004) is chosen to solve the SW equations. In particular, the numerical fluxes $F_{j+1/2L,R}$ were derived using a hydrostatic reconstruction technique. This scheme allows to preserve a particular steady state of (11) called lake at rest, *i.e.* $h + z_b = \text{const.}$ and $u = 0$. Nevertheless, it has difficulties to deal with a combination of large bottom slopes and a small water depth (*Delestre et al.*, 2012). A recent modification in *Berthon and Foucher* (2012) allows this limitation to be overcome.

Given the discrete data $(U_j^n, U_{j+1}^n, \Delta z_{bj+1/2})$, the scheme based on the hydrostatic reconstruction technique carries out the two following steps:

1. computation of the reconstructed states $U_{j+1/2L,R}$ at the interface

$$\begin{aligned} h_{j+1/2L} &= \max(0, h_j^n - \max(0, \Delta z_{bj+1/2})), \\ h_{j+1/2R} &= \max(0, h_{j+1}^n + \min(0, \Delta z_{bj+1/2})), \\ U_{j+1/2L} &= (h_{j+1/2L}, h_{j+1/2L} u_j^n)^t, \\ U_{j+1/2R} &= (h_{j+1/2R}, h_{j+1/2R} u_{j+1}^n)^t, \end{aligned}$$

2. construction of the numerical fluxes from the reconstructed states obtained before

$$\begin{aligned} F_{j+1/2L} &= \mathcal{F}(U_{j+1/2L}, U_{j+1/2R}) + \left(0, \frac{g}{2}(h_j^2 - h_{j+1/2L}^2)\right)^t, \\ F_{j+1/2R} &= \mathcal{F}(U_{j+1/2L}, U_{j+1/2R}) + \left(0, \frac{g}{2}(h_{j+1}^2 - h_{j+1/2R}^2)\right)^t, \end{aligned}$$

   where $\mathcal{F}(U_{j+1/2L}, U_{j+1/2R})$ is a consistent numerical flux for the homogeneous SW equations. In this work, we adopted the HLL formulation (*Harten et al.*, 1983) for $\mathcal{F}(U_{j+1/2L}, U_{j+1/2R})$. According to *Batten et al.* (1997), an appropriate choice for the wave speed estimates can lead the HLL Riemann solver to satisfy automatically an entropy inequality, to resolve isolated shocks exactly, and to preserve positivity. When both sides of the cell interface are wet, a natural choice is to compare the maximum and minimum characteristics velocities evaluated at both left and right given states. These estimates can also be improved using the Roe average. For the wet/dry transitions, a more suitable estimation for the wave speeds can be derived from the exact Riemann solution (*Toro*, 2001). Consequently, the resulting scheme preserves the positivity and is well adapted to wet/dry transitions[1].

[1]The detailed method have been implemented in FullSWOF_2D, see `https://sourcesup.renater.fr/projects/fullswof-2d/`

### 3.1.2 A new approach for the sediment transport

An important remark is that, in equation (10), the sediments are simply convected by the water flow. At the numerical level, contrary to *Heng et al.* (2009); *Kim et al.* (2013), we choose an upwind scheme to solve equation (10) linking the transport of sediment to the SW equations

$$\overline{(ch)}_j := \overline{c}_j \overline{h}_j = c_j^n h_j^n - \frac{\Delta t}{\Delta x}\left(F_{j+1/2}^{ch} - F_{j-1/2}^{ch}\right). \tag{17}$$

The related upwind flux $F_{j+1/2}^{ch}$ for sediment transport is given by

$$F_{j+1/2}^{ch} = \begin{cases} c_j^n F_{j+1/2}^h & \text{if } F_{j+1/2}^h > 0, \\ c_{j+1}^n F_{j+1/2}^h & \text{else,} \end{cases} \tag{18}$$

where $F_{j+1/2}^h$ is the numerical flux given by (13).

An important property of the scheme (17) is that the positivity of the sediment concentration $\overline{c}_j$ is *automatically* preserved under the CFL condition (14) of the SW equations. In fact, denoting $F_{j+1/2}^+ = \max(F_{j+1/2}^h, 0)$ and $F_{j+1/2}^- = \min(F_{j+1/2}^h, 0)$, we have $F_{j+1/2}^h = F_{j+1/2}^+ + F_{j+1/2}^-$ and $F_{j+1/2}^{ch} = c_j^n F_{j+1/2}^+ + c_{j+1}^n F_{j+1/2}^-$. The scheme (17) can be rewritten as

$$\begin{aligned} \overline{c}_j \overline{h}_j &= c_j^n h_j^n - \frac{\Delta t}{\Delta x}\Big(c_j^n (F_{j+1/2}^+ - F_{j-1/2}^-) \\ &\quad + c_{j+1}^n F_{j+1/2}^- - c_{j-1} F_{j-1/2}^+\Big) \\ &= c_j^n \left(h_j^n - \frac{\Delta t}{\Delta x}\left(F_{j+1/2}^+ - F_{j-1/2}^-\right)\right) \\ &\quad + c_{j-1}^n \left(\frac{\Delta t}{\Delta x} F_{j-1/2}^+\right) - c_{j+1}^n \left(\frac{\Delta t}{\Delta x} F_{j+1/2}^-\right) \\ &= c_{j-1}^n \alpha_{j-1} + c_j^n \alpha_j + c_{j+1}^n \alpha_{j+1}, \end{aligned} \tag{19}$$

and we notice from equation (15) that $\alpha_{j-1} + \alpha_j + \alpha_{j+1} = \overline{h}_j$. Let us assume for the moment that $\alpha_{j-1}, \alpha_j, \alpha_{j+1} \geq 0$. We deduce, by dividing equation (19) by $\overline{h}_j$, that $\overline{c}_j$ is a convex combination of $c_{j-1}^n, c_j^n$ and $c_{j+1}^n$. Hence, we have the following inequalities also known as the discrete maximum principle

$$\min(c_{j-1}^n, c_j^n, c_{j+1}^n) \leq \overline{c}_j \leq \max(c_{j-1}^n, c_j^n, c_{j+1}^n).$$

In particular, given $c_{j-1}^n, c_j^n, c_{j+1}^n \geq 0$, the updated sediment concentration $\overline{c}_j$ is non-negative.

The only remaining problem concerns the non-negativity of $\alpha_{j-1}, \alpha_j, \alpha_{j+1}$. We have immediately $\alpha_{j\pm1} \geq 0$ from the definition of $F_{j+1/2}^{\pm}$. On the non-negativity of $\alpha_j$, we rewrite

$$\begin{aligned} \alpha_j &= \frac{1}{2}\left(h_j^n - \frac{2\Delta t}{\Delta x}\left(F_{j+1/2}^+ - h_j^n u_j^n\right)\right) \\ &\quad + \frac{1}{2}\left(h_j^n - \frac{2\Delta t}{\Delta x}\left(h_j^n u_j^n - F_{j-1/2}^-\right)\right). \end{aligned}$$

It is enough to check that each of these two terms is non-negative. In the case when $F_{j-1/2}^- = 0$ or $F_{j+1/2}^+ = 0$, the corresponding term reduces to $\frac{1}{2} h_j^n \left(1 \pm \frac{2\Delta t}{\Delta x} u_j^n\right)$ which is non-negative under the CFL condition (14) because $|u_j^n| \leq \max(|s_L|, |s_R|)$. In the opposite case, the non-negativity of these terms is guaranteed by the property (16) of the numerical fluxes $F_{j+1/2L,R}$.

### 3.2 Source terms discretization

At the end of the convective step, we obtain the state $\overline{\mathbf{U}}$ from the given value $\mathbf{U}^n$ via the well-balanced scheme (12) and the upwind scheme (17). The next step is to compute the contribution of the source terms $S_1,\ S_2$. This step consists in the resolution of mentioned ODE system to obtain $(\mathbf{U}, \mathbf{V})^{n+1}$ from the initial value $(\overline{\mathbf{U}}, \mathbf{V}^n)$.

The water source and friction terms are treated as in *Delestre et al.* (2014). The rain and the infiltration terms are treated explicitly as they involve no particular numerical difficulties such as steady-state or stability requirements. In FullSWOF_2D, the infiltration rate is computed by the Green-Ampt model (*Green and Ampt*, 1911). Concerning the friction terms, FullSWOF_2D uses a semi-implicit discretization (as in *Bristeau and Coussin*, 2001; *Liang and Marche*, 2009; *Delestre et al.*, 2014) to preserve the stability when simulations involve wet/dry fronts, and to keep the well-balanced property obtained in the convective step.

Let us turn to the main difficulty brought by the source terms: the contributions of erosion and deposition given by system (3). This system expressing the HR model for $I$ sediment classes can be rewritten as the following equations, for $i = 1, \dots, I$:

$$\partial_t(c_i h) = e_i + e_{ri} + r_i + r_{ri} - d_i, \tag{20}$$

$$\partial_t m_i + \partial_t(c_i h) = e_i + r_i, \tag{21}$$

$$\rho_s(1-\phi)\partial_t z_b + \sum_{i=1}^{I} \partial_t(c_i h) = 0. \tag{22}$$

System (20)–(22) can be computed directly by using an explicit Euler's method. Nevertheless, it requires a special treatment for each situation called *before-ponding* and *after-ponding* that correspond to two different behaviours of erosion processes. These cases are differentiated numerically by a small artificial threshold $h_p$ of the water depth.

#### 3.2.1 Classical approach for erosion and deposition, modifying the CFL condition

We detail here how equations (20)–(22) have been discretized, depending on the erosion process.
**Before-ponding.** When $h \leq h_p$, the detached sediments are not transported but accumulate into the deposited layer on the soil surface. Equations (20)–(22) reduce to $\partial_t m_i = e_i$. This situation is treated numerically, as mentioned in *Heng et al.* (2011), by setting

$$(c_i h)^{n+1} = 0,$$
$$(m_i)^{n+1} = (m_i)^n + \overline{(c_i h)} + \Delta t (e_i)^n.$$

**After-ponding.** When $h > h_p$, the detached sediments can be suspended in flow. Physically, the amount of sediment deposited over a time increment cannot be greater than that in the flow. While the positivity of sediment concentration is well preserved in the convective step, this is no longer evident when using an explicit approximation to solve equations (20)–(22). That is the reason why, in *Heng et al.* (2009), an additional restriction on the time step has been introduced, namely

$$\Delta t \leq \left(\frac{c_i h}{d_i}\right)^n = \frac{h^n}{v_{fi}}, \quad \text{for } i = 1, \dots, I. \tag{23}$$

In *Kim et al.* (2013), a small improvement has been made by only checking (23) on wetted regions where the detached particles can be transported in suspension. This allows to avoid the fact that

$\Delta t \to 0$ during the pre-ponding period. Equation (23) becomes

$$\Delta t \leq \frac{\min_{j=1,2,\ldots,N_c} h_j^n}{\max_{i=1,2,\ldots,I} v_{fi}},$$

where $N_c$ is the number of wetted cells of the mesh. All these authors found that for small water depths, the time step $\Delta t$ is governed by this additional restriction rather than by the CFL condition (14) of the SW equations.

### 3.2.2 A new approach for erosion and deposition, with an unchanged CFL condition

We notice that the additional restriction (23) on the time step raises from the use of explicit discretization for equation (20). To relax this limitation, we can solve numerically this equation in two successive steps consisting of $(i)$ the phase of deposition and $(ii)$ the phase of erosion

$$\begin{aligned} (i) \quad & \partial_t(c_i h) = -d_i = -\frac{v_{fi}}{h}(c_i h), \\ (ii) \quad & \partial_t(c_i h) = e_i + e_{ri} + r_i + r_{ri}. \end{aligned}$$

Since the water depth remains constant in these steps, the advantage of this fractional method is that the first equation can be solved analytically while an explicit discretization can be used for the second one. Hence we replaced the classical approach by using the Strang-splitting method (see e.g. *McLachlan and Quispel*, 2002) to solve (20). This consists to compute sequentially $(i)$ with a haft time step $\Delta t/2$, next $(ii)$ with full time step $\Delta t$ and lastly $(i)$ again with $\Delta t/2$. Given an initial state $\overline{(c_i h)}$, the resulting scheme writes

$$\begin{aligned} \overline{\overline{(c_i h)}} &= \exp\left\{-\frac{v_{fi}}{\overline{h}}\frac{\Delta t}{2}\right\}\overline{(c_i h)}, \\ \overline{\overline{\overline{(c_i h)}}} &= \overline{\overline{(c_i h)}} + \Delta t(e_i + r_i)^n + \Delta t(e_{ri} + r_{ri})^n, \\ (c_i h)^{n+1} &= \exp\left\{-\frac{v_{fi}}{\overline{h}}\frac{\Delta t}{2}\right\}\overline{\overline{\overline{(c_i h)}}}. \end{aligned} \tag{24}$$

The proposed scheme presents several advantages. Firstly, equation (24) is computed as second order accurate and therefore achieves the accuracy required of the overall scheme. Secondly, as the Strang-splitting is symmetric, the deposition process is treated both before and after erosion. This allows the scheme to maintain the simultaneous nature of the erosion and deposition of these processes.

Another remark at the numerical level is that while $(e_i + r_i)^n$ can be computed directly from equations (2), (4), the quantity $\Delta t \sum_{i=1}^{I}(e_{ri} + r_{ri})^n$ may not be greater than $(m_T)^n$. Indeed $\Delta t \sum_{i=1}^{I}(e_{ri} + r_{ri})^n$ is the quantity of sediment available for re-detachment and re-entrainment. From equations (3) and (5), we define $(e_r + r_r)^n$ at each instant $t^n$ as the total capacity of re-detachment and re-entrainment from the deposited layer

$$(e_r + r_r)^n = H\left(a_d R + \frac{F(\omega - \omega_{cr})}{\frac{\rho_s - \rho_w}{\rho_s} g h}\right).$$

The total rate of re-detachment and re-entrainment of the sediment class $i$ is given by

$$\Delta t(e_{ri} + r_{ri})^n = \frac{(m_i)^n}{(m_T)^n} \min\left\{(m_T)^n, \Delta t(e_r + r_r)^n\right\}. \tag{25}$$

The scheme (24) together with (25) shows that $(c_i h)^{n+1} \geq 0$ since $\overline{(c_i h)} \geq 0$ (obtained from the upwind scheme (17)). The positivity of $c_i$ is thus preserved without requiring the supplementary condition (23) on the time step.

Using (24), we can now solve, in a conservative way, equations (21)–(22) to obtain the mass of deposited layer and the topography at time $t^{n+1}$

$$\begin{aligned} (m_i)^{n+1} &= (m_i)^n + \Delta t (e_i + r_i)^n - \left( (c_i h)^{n+1} - \overline{(c_i h)} \right), \\ (z_b)^{n+1} &= (z_b)^n - \frac{1}{\rho_s (1-\phi)} \sum_{i=1}^{I} \left( (c_i h)^{n+1} - \overline{(c_i h)} \right). \end{aligned} \tag{26}$$

Let us summarise the main properties of proposed method. The numerical scheme combining (12)–(17), (24), (26) is conservative, well-balanced, positivity preserving for both of the water depth and the sediment concentration. In particular, only the CFL condition of the SW equations is required to ensure the stability of the overall numerical scheme.

# 4 Numerical results

As explained before, the proposed model is a coupling between the SW equations and the HR model. We thus use a SW code, to which we add an erosion component. For the SW part, we use the C++ code *FullSWOF* (Full Shallow Water equations for Overland Flow). This software, developed in the framework of the multi-disciplinary project METHODE ANR-07-BLAN-0232, is distributed under CeCILL-V2 (GPL compatible) free software license, and available at `http://www.univ-orleans.fr/mapmo/soft/FullSWOF/`, see *Delestre et al.* (2014). The resolution of the SW equations can be performed at second order in time and space using the MUSCL reconstruction and the hydrostatic reconstruction, as noted in the previous section.

In this section, we present numerical validations of the proposed approximation for system (1) coupling the SW equations to the HR model, using equations (12)–(17), (24), (26). Unfortunately, there is no time and space-dependent analytic solution available for this system. So we validate separately the convective part, modelling overland flow and sediment transport, and the HR model describing the processes of erosion and deposition. As the convective step has been developed on the basis of *FullSWOF*, we do not need to perform any numerical validations for the hydrodynamic part, since this has previously been done by *Delestre et al.* (2013, 2014) for various benchmark tests. After these series of tests for the validation of the numerical method, we give a two-dimensional example on a real topography for which we compare the maximum-allowed time step of CFL condition (14), and that of condition (23).

## 4.1 Tests on the convective step for the sediment transport

In order to test the new part of the convective step (equation (17)), it is necessary to cancel the erosion and deposition processes to impose $S_1 = S_2 = 0$; for this, it is sufficient to set $S_f = a = a_d = v_f = 0$.

We aim at testing two important properties of this numerical scheme computing the evolution of sediment concentration in shallow flow: the consistency and the preservation of equilibria. We perform two test cases proposed in *Audusse and Bristeau* (2003) for the transport of a passive pollutant by the flow.

### 4.1.1 Dam break on a flat bottom with sediments

This classical test simulates the case of a dam break on a flat bottom with no friction, in which the concentration of sediment is different at each side of the dam. In other words, the configuration of this test is exactly the Riemann problem of the homogeneous system of (8, 9, 10). We consider a spatial domain of length 2000 m, discretized by an uniform mesh with 100 cells, and we set the final time of simulation to $T = 240$ s. The dam is located at the center of the domain, that is at $x_0 = 1000$ m. For the initial conditions, we set $h_l = 1,\ q_l = 0,\ c_l = 0.7$ on the left boundary, and $h_r = 0.5,\ q_r = 0,\ c_r = 0.5$ on the right boundary.

The interest of this test is that we have an expression of the exact solution (see *Stoker*, 1957). From left to right, the solution is separated by two constant intermediate states. The first one connects to the left given state by a rarefaction wave propagating with a speed $u - \sqrt{gh}$. The second one connects to the right given state by a shock wave propagating with a speed $u + \sqrt{gh}$. These intermediate states are separated by a discontinuity wave propagating with the flow speed. Recall that in the exact solution, the values of $h$ and $u$ do not change across the contact waves in the intermediate region, while the concentration $c$ transported with the flow does not change across the non-linear waves but changes, discontinuously, across the contact wave. To check the convergence property of the proposed method, we perform this test with the first and second order schemes.

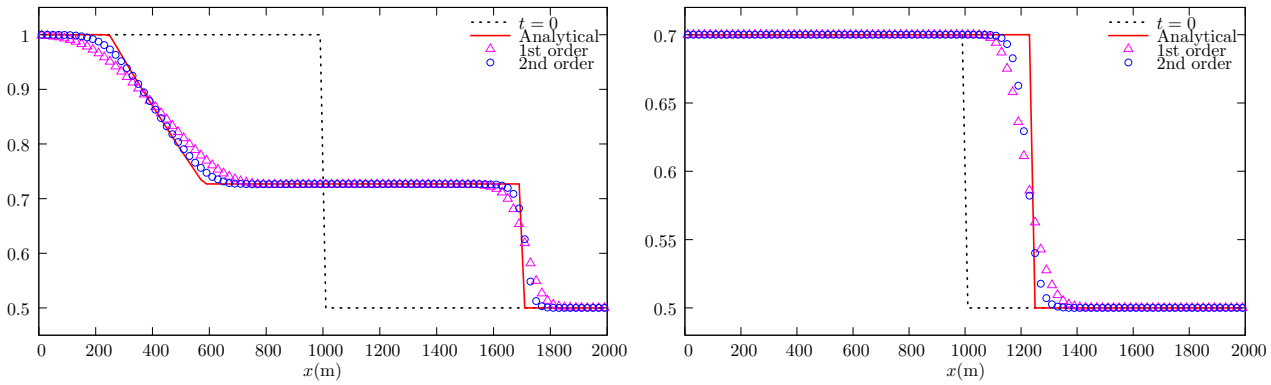


Figure 2: Dam break: water depth (left) and sediment concentration (right) at $T = 240$ s.

In Fig. 2, we plot the initial condition (dotted line), the analytic solution (continuous line), the first order approximation (triangles) and the second order approximation (circles) for the water depth and the sediment concentration. The numerical results show that the analytic solution is approximated well and that the second order is, as expected, a better approximation.

### 4.1.2 Preservation of the steady state of the lake at rest

Next we want to verify numerically the steady state of the lake at rest. In this case, the equilibrium of the concentration must be also preserved. So we use a non-flat bottom

$$z_b(x) = \begin{cases} 0 & \text{if } 0 \leq x < 8, \\ 0.2 - 0.05(x-10)^2 & \text{if } 8 \leq x \leq 12, \\ 0 & \text{if } 12 < x \leq 20 \end{cases}$$

discretized by a uniform mesh with 100 cells. The initial condition is

$$h(0,x) + z_b(x) = 1, \quad u(0,x) = 0, \quad \text{and} \quad c(0,x) = \begin{cases} 0 & \text{if } 0 \le x < 8, \\ 1 & \text{if } 8 \le x \le 10, \\ 0 & \text{if } 10 < x \le 20. \end{cases}$$

Note that the initial condition of $h$ and $u$ satisfies the equilibrium of the lake at rest. Moreover, the sediment flux is zero since $hu = 0$, which means that the given sediment concentration is maintained in the exact solution. From the well-balancing condition of the numerical fluxes $F_{j+1/2L,R}$, we have $F^h_{j+1/2} = h^n_j u^n_j = 0$ and so the numerical flux of sediment transport $F^{ch}_{j+1/2} = 0$ by definition (18). Consequently, the given sediment concentration is also preserved at numerical level. This is an interesting feature of the upwind scheme (17).

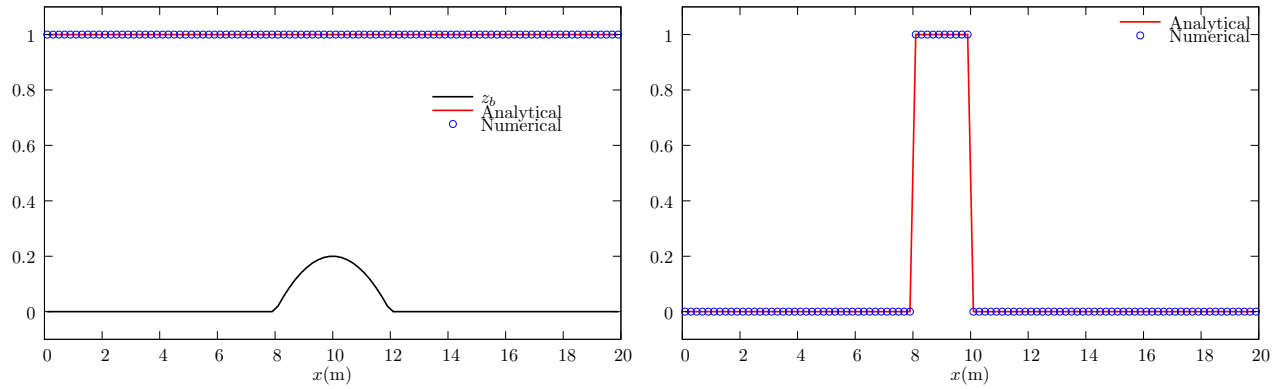


Figure 3: Lake at rest: free surface elevation (left) and sediment concentration (right).

We present in Fig. 3 the numerical results after 100 s, for the free surface elevation and the sediment concentration. In both results, the stationary solution is preserved exactly.

## 4.2 Tests with some specific solutions of HR model

After the numerical tests on the convective step, let us check the functionality of the erosion and deposition steps, approximated by schemes (24)–(26). In the literature, some analytic, semi-analytic or numerical solutions are available for the HR model with specific assumptions (*Sander et al.*, 1996, 2002; *Hairsine et al.*, 2002; *Hogarth et al.*, 2004; *Rose et al.*, 2007; *Barry et al.*, 2010). Here, we compare our numerical results with two reference solutions proposed by *Sander et al.* (2002) and *Hogarth et al.* (2004) as these solutions have shown a good agreement with experiments.

### 4.2.1 A steady state analytic solution: net deposition in overland flow

In this section, we are interested in a special configuration which results in a net deposition region. It is the zone where the sediment flux decreases downslope and the deposited layer develops very rapidly to completely shield the original soil (so the shielding factor $H \approx 1$). We also assume that the water flow is deep enough (greater than 3 drop diameter), allowing us to neglect the re-detachment process by rainfall. Indeed the impact of raindrops in that case is largely absorbed by the water layer. Hence re-entrainment and deposition are the only active erosion mechanisms. The equations of mass

conservation of sediment reduce to

$$\partial_t(c_i h) + \partial_x(c_i q) = r_{ri} - d_i,$$
$$\partial_t m_i = d_i - r_{ri}.$$

*Hairsine et al.* (2002) presented a steady state single-class analytic solution when there is no rainfall and a constant flow rate imposed at the top of slope, *i.e.* $q = q_0 = \text{const}$. *Sander et al.* (2002) extended the solution to the case of multi-size classes. Their solution is

$$\begin{aligned} c_i(x) &= c_{i0}\left(\frac{c_I(x)}{c_{I0}}\right)^{\frac{v_{fi}}{v_{fI}}}, \quad \text{for } i = 1, 2, \ldots, I-1, \\ m_i(t,x) &= v_{fi} c_i(x)\left(1 - \frac{\gamma^*}{\sum_{i=1}^{I} v_{fi} c_i(x)}\right) t, \ \text{for } i = 1, \ldots, I, \end{aligned} \tag{27}$$

where $c_{i0}$ is the concentration of the sediment class $i$ upstream and

$$\gamma^* = \gamma q_0^{2/5}\left(1 - \frac{q_{cr}}{q_0}\right), \quad \gamma = \frac{F\rho_s\rho_w S K^{3/5}}{\rho_s - \rho_w}$$

with $K = \dfrac{\sqrt{S}}{\mathrm{n}}$, $q_{cr} = \dfrac{\omega_{cr}}{\rho_w g S}$ and $S$ is the bottom slope. Finally, the concentration $c_I(x)$ of the last sediment class can be computed analytically by solving the following equation

$$\frac{dc_I(x)}{dx} = \left(\frac{\gamma^*}{\sum_{i=1}^{I} v_{fi} c_{i0}\left(\frac{c_I}{c_{I0}}\right)^{\frac{v_{fi}}{v_{fI}}}} - 1\right)\frac{v_{fI} c_I}{q_0}$$

which leads to

$$\int_{c_{I0}}^{c_I(x)} \left(\frac{\gamma^*}{\sum_{i=1}^{I} v_{fi} c_{i0}\left(\frac{\bar{c}_I}{c_{I0}}\right)^{\frac{v_{fi}}{v_{fI}}}} - 1\right)^{-1} \frac{d\bar{c}_I}{\bar{c}_I} = \frac{v_{fI}}{q_0} x. \tag{28}$$

We perform this benchmark with the parameters used in *Heng et al.* (2009):

- hydraulic parameters: $S = 0.02$, $\mathrm{n} = 0.01$, $q_0 = 0.00125$ m$^2$/s.
- erosion parameters: 10 classes of sediments of a soil in the loam belt of central Belgium; $v_{fi}$ (in mm/s) are taken from experimental data of *Beuselinck et al.* (1999): 0.00043, 0.0037, 0.02, 0.083, 0.23, 0.46, 0.74, 1.1, 1.7, and 3.2 respectively; $\rho_s = 2600$ kg/m$^3$, $F = 0.01$, $\omega_{cr} = 0.186$ W/m$^2$.
- boundary condition: $c_{i0} = 10$ kg/m$^3$, for $i = 1, \ldots, I$.
- initial condition: $c_i(0, x) = 10$ kg/m$^3$, for $i = 1, \ldots, I$.

Fig. 4 presents the numerical results with $\Delta t = 0.05$s and 100 cells, at time $T = 10$ min, in order to reach the steady state. More precisely, the sediment concentrations for the classes numbered 1, 4, 7, 9 and 10 are plotted as functions of the space variable. One can note that the numerical and analytic results are similar.

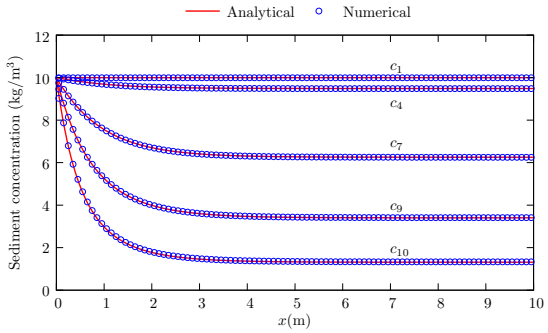


Figure 4: Net deposition in overland flow.

#### 4.2.2 A transitory solution: rainfall-driven erosion

This benchmark is a case where the solution is time-dependent. However, there is no such analytic solutions available in literature for the coupled system SW-HR. The solution, proposed by *Hogarth et al.* (2004), is derived from the system coupling the kinematic wave model (*Woolhiser and Liggett*, 1967) and the HR model. This numerical solution of rainfall-driven erosion describes the dynamics of sediment eroded by rainfall impacts when there is no inflow of water at the top of the eroded slope, and no infiltration of water in the soil. This solution allows us to investigate the variation of sediment concentration as a function of time, downslope distance and settling velocity.

Contrary to the previous test, the flow-driven processes are not present in the configuration of this benchmark and the rainfall impact is the only erosion agent. The mass conservation equations of HR model reduce to

$$\begin{aligned}\partial_t(c_i h) + \partial_x(c_i q) &= e_i + e_{ri} - d_i,\\ \partial_t m_i &= d_i - e_{ri}.\end{aligned}$$

Considering a stationary solution of the kinematic model with no inflow, and assuming that in the original soil, each class contains an equal mass of sediment, *i.e.* $p_i = 1/I$. A numerical solution was computed by using a semi-implicit upwinding finite difference method which lead to the following scheme after rearranging

$$\begin{aligned}(c_i)_j^{n+1} =& \left(1 - \frac{\lambda q}{h} - \frac{\kappa}{h}\left(1 + \frac{v_{fi}}{R}\right)\right)(c_i)_j^n + \frac{\lambda q}{h}(c_i)_{j-1}^n \\ &+ \frac{\kappa}{h}\left(\beta(m_i)_j^{n+1} + \frac{a}{I}\left(1 - \frac{\sum_{i=1}^{I}(m_i)_j^{n+1}}{m_T^*}\right)\right), \qquad (29)\\ (m_i)_j^{n+1} =& (1-\kappa\beta)(m_i)_j^n + \frac{\kappa v_{fi}}{R}(c_i)_j^n.\end{aligned}$$

where $\lambda = \Delta t/\Delta x$, $\kappa = R\Delta t$ and $\beta = a_d/m_T^*$. An initial condition (at $t = 0$) and a boundary condition (at the upstream $x = 0$) for each sediment class $i = 1, \ldots, I$ are required to close the scheme (29)

$$\begin{aligned}\text{initial condition:} \quad & (c_i)_j^0 = 0, \quad (m_i)_j^0 = 0,\\ \text{boundary condition:} \quad & (c_i)_0^n = 0, \quad (m_i)_0^n = 0.\end{aligned}$$

We perform this last benchmark with the parameters used in *Heng et al.* (2009):

- domain setting: $L = 5.8$ m discretized by 100 cells, $\Delta t = 0.002$ s;
- hydraulic parameters: $S = 0.004$, n $= 0.06$, R $= 100$ mm/h;
- erosion parameters: 10 classes of sediment with $v_{fi}$ (in mm/s) $= 0.21$, 0.71, 3.3, 10.9, 19.4, 31.2, 69.1, 139, 210, and 300 respectively; $a = 920$ kg/m$^3$, $a_d = 14190$ kg/m$^3$, $m_T^* = 0.0767$ kg/m$^2$.

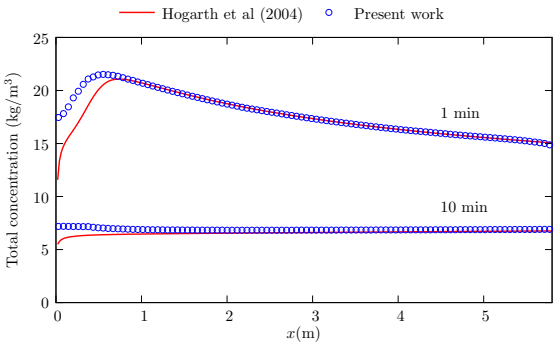


Figure 5: Rainfall-driven erosion.

On Fig. 5 we plot, for two different times, the variations in space of the total sediment concentration obtained by our new method, coupling the SW system and the HR model, and the approximation of the analytic solution of the kinematic wave coupled with HR model, given by equation (29). We find again a good agreement between the two solutions, the difference on the left part of the domain lying in the difference between the SW and the kinematic wave models. We also obtain good results compared to experiment observations of *Proffitt et al.* (1991): sediment concentration decreases with time until the steady-state concentration is reached.

### 4.3 A two-dimensional test case

The previous one-dimensional tests using analytic solutions justify the important properties of proposed method such as convergence and preserving steady state. Before entering into our last experiment, it is important to keep in mind that the present objective is not to validate the physical model (1) since this has been investigated in several publications. For plot-scale, *Heng et al.* (2011) found a good agreement with experiment on the dynamics of sediment concentration and the particle size distribution. Recently, *Kim et al.* (2013) obtained satisfactory results at catchment-scale with the simulation using the database of the Lucky Hills watershed (located in southeastern Arizona, USA). Moreover, in-depth discussions on the parameters can be found in *Heng et al.* (2011) and *Kim and Ivanov* (2014). We perform here a two-dimensional simulation with a realistic irregular topography taking into account the erosion and deposition effects. The chosen configuration includes wet/dry fonts, water infiltration and rainfall-driven erosion processes with multiple sediment classes. On one hand, this test case allows us to check the good coherence of the proposed solver. On the other hand, it allows us to emphasize the gain in computational time of our method.

We use the database collected on the plot of Thies (Senegal) realized by IRD (*Tatard et al.*, 2008) in the project PNRH RIDES. The dataset is freely available at `http://www.umr-lisah.fr/Thies_2004/`. The plot was 10 m long by 4 m wide, with a 1% slope, and sandy soil (1% clay, 7% silt, 43% fine sand, 49% coarse sand). The surface was raked in order to form a slight V shape, with 1% slope

longitudinally and 1% transverse slope. The purpose of the V shape was to avoid rill development at the lateral boundaries of the plot. A 2-hour long rainfall event was applied at a constant intensity of 70 mm/h in order to maintain a steady runoff and infiltration rate. See *Mügler et al.* (2011) for more details on the experimental design. The granulometry of the sandy soil is given in Table 1 and the related settling velocities of 10 classes of sediment are calculated using Cheng's formula (*Cheng*, 1997).

| Grain size ($\mu$m) | 10 | 20 | 50 | 100 | 150 | 200 | 250 | 500 | 750 | 1000 |
|---|---|---|---|---|---|---|---|---|---|---|
| Proportion (%) | 1 | 2 | 4 | 13 | 15 | 14 | 13 | 32 | 5 | 1 |
| Settling velocity (mm/s) | 0.04 | 0.16 | 1 | 3.8 | 7.8 | 12.6 | 17.8 | 43.1 | 64.6 | 82.1 |

Table 1: Granulometry of the sandy soil.

The plot surface was dry at the beginning of simulation while the sandy soil was considered as completely cohesive. The friction term is calculated by the Darcy-Weisbach's formula and the infiltration rate is given by the Green-Ampt model. Details on the parameters for the SW equations can be found in *Delestre et al.* (2014). An associated ponding depth $h_p = 1.5d_s$ was set for each grain size $d_s$. By regarding the range of grain sizes in table 1, this setting allows us to simulate simultaneously *before-* and *after-ponding* situations between the different sediment classes and in particular during transition periods. According to the discussion in *Heng et al.* (2011), other parameters of the HR model are chosen as: $F = 0.1$, $\omega_{cr} = 0.1525$ W/m$^2$, $J = 100$ J/kg, $h_0 = 0.66 \times 10^{-3}$ m, $b = 1$, $a_0 = 150$ kg/m$^3$, $a_{d0} = 1500$ kg/m$^3$ and $m^*_{T0} = 1$ kg/m$^2$.

The simulation result at the end of rainfall even ($t = 120$ mn) is shown in Fig. 6. Except for the main flow located in the rill, the flow is very shallow ($h \sim 1$mm) as most of the water has infiltrated (Fig. 6a). Moreover, the water flux (Fig 6b) is nearly negligible except at the outlet, so the stream power is unlikely to exceed its critical value. This means that the flow has no contribution from sediment entrainment but just caries the detached particles. Consequently, the chosen configuration is typically rainfall-driven erosion. Fig. 6c, presenting the mass of deposited layer, showed that in large regions of the plot, rainfall detachment accumulates soil particles into a non-cohesive (deposited) layer and the related critical value was rapidly reached. In the main flow where the thickness of water layer is sufficiently important, *i.e.* $h \gg h_0$, rainfall erosivity is limited since the raindrop energy is reduced as it penetrates the surface water layer.

Particle size-selectivity characteristics are shown in Fig. 6d,e,f. As the flow is very shallow, we pay attention particularly on the fine grains ($d_s \leq 100\mu$m), for example silt and fine-sand. Fig. 6d-e show that the 1st class ($d_s \leq 10\mu$m) and the 2nd class ($d_s \leq 20\mu$m) occupy an important factor in the total concentration of sediment in flow while it was initially only 1% and 2% in original soil. On the contrary, the 4th class ($d_s \leq 10\mu$m) is nearly absent in the main flow as opposed to their significant proportion (13%) in original soil (Fig. 6f).

Let us check an advantage of the proposed scheme relating on the computational efficiency. Recall that only the CFL condition of the SW equations is required while an additional condition of HR equations must be used in the approach of *Heng et al.* (2009) and *Kim et al.* (2013). Fig. 7 presents the maximum-allowed time steps given by conditions (14) and (23). During transition period (first 10 minutes of rainfall event), the condition (23) is very restrictive contrary to what happens for the SW equations. When the flow reaches steady state, the time step of SW equations is in order of $10^{-2}s$ and two orders of magnitude higher than that of the HR equations ($10^{-4}s$). Consequently, the condition (23) is at least 100 times more restrictive than (14). It is important to recall a well-known numerical effect which states that the more the timestep is reduced, the more numerical diffusion is added.

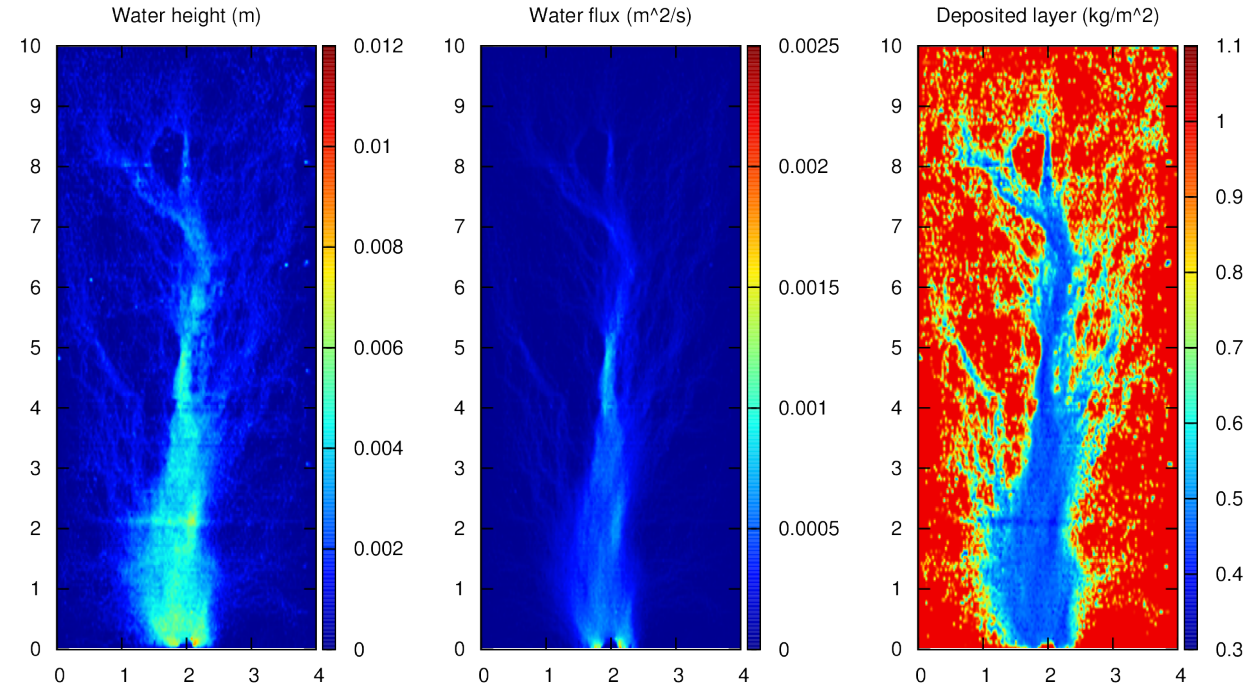


(a) (b) (c)

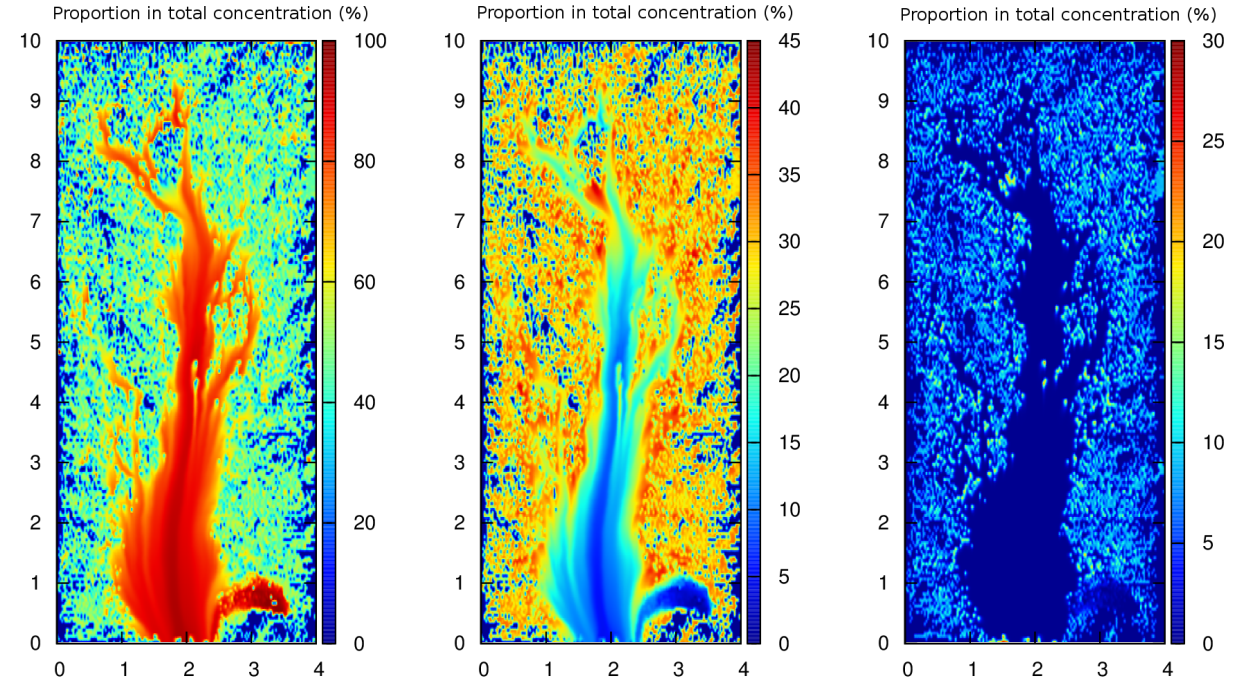


(d) $d_s = 10\mu$m (e) $d_s = 20\mu$m (f) $d_s = 100\mu$m

Figure 6: Simulation result at $t = 120$ minutes

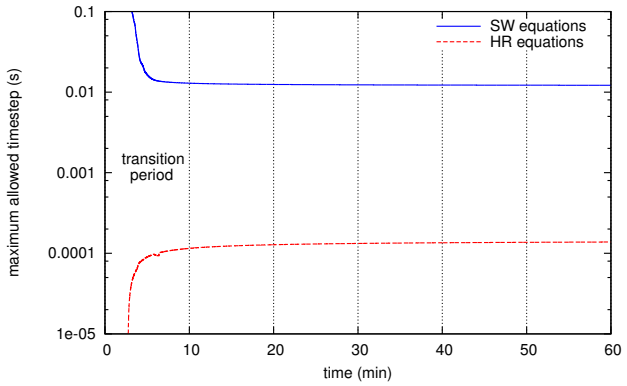


Figure 7: Gain in performance by using large timestep

# 5 Conclusion

The system coupling of the SW equations with the HR model allows the simulation of complex scenarios of soil erosion by rainfall and overland flow on a non-uniform topography. This model predicts not only the topographical evolution and the eroded sediment flux but also the particle-selectivity during erosion processes. *Heng et al.* (2009) and *Kim et al.* (2013) proposed numerical finite volume methods for one and two-dimensional systems. These schemes are based on Roe's approximate of Riemann solvers in which an additional restriction on the time step is required together with the classical CFL condition of the SW equations in order to ensure the positivity of the sediment concentration.

We have proposed an alternative numerical finite volume solver in which $(i)$ the approximation of erosion part is less dependent on the numerical approximation of the hydrodynamics; $(ii)$ only the CFL condition associated to the SW equations is sufficient to ensure the stability of numerical solution. It has been shown that the present method is well-balanced and positivity preserving. The numerical approximation for the erosion part can be adapted to any well-balanced and positivity preserving approximation of the SW equations. This offers more possible solutions in the choice of numerical solvers for the hydrodynamic component, especially the recent and advanced approaches published in the last few years. In terms of performance, the scheme allows larger time steps than those required by *Heng et al.* (2009); *Kim et al.* (2013) and consequently offers a more efficient solution. A two-dimensional test on a realistic topography shows that the computation is at least 100 times faster due to the proposed new solver. Finally in each time step, the computation corresponding to each sediment class is independent of each other and thus can be performed in parallel (for example with OpenMPI). This property becomes interesting when we deal with a large number of sediment classes.

# Table of notations

| | |
|---|---|
| $a,\ a_0$ | detachabilities of original soil. |
| $a_d,\ a_{d0}$ | detachabilities of deposited layer. |
| $b$ | exponent used in equation (7). |
| $c_i$ | mass sediment concentration. |
| $d_i$ | deposition rate. |
| $d_s$ | particle size. |

| | |
|---|---|
| $e_i,\ e_{ri}$ | rainfall detachment, re-detachment rates. |
| $f$ | Darcy-Weisbach friction factor. |
| $F$ | effective fraction of excess stream power. |
| $g$ | gravitational acceleration. |
| $h$ | flow depth. |
| $H$ | fractional shielding of original soil. |
| $h_0$ | threshold depth used in equation (7). |
| $h_p$ | ponding depth. |
| $i$ | particle size class index. |
| $j$ | cell index in the mesh. |
| $I$ | number of sediment size classes. |
| $I_r$ | rate of infiltration. |
| $J$ | specific energy of sediment. |
| $m_i$ | mass of the $i$-th class in deposited layer. |
| $m_T$ | accumulated mass per unit area of deposited layer. |
| $m_T^*$ | deposited mass required to shield original soil. |
| n | Manning friction factor. |
| $p_i$ | proportion of the $i$-th class in original soil. |
| $R$ | rainfall intensity. |
| $r_i,\ r_{ri}$ | flow entrainment, re-entrainment rates. |
| $S$ | bottom slope. |
| $S_f$ | friction slope. |
| $S_0,\ S_1,\ S_2$ | vectors of source terms. |
| $s_L,\ s_R$ | wave speeds related to the SW equations. |
| $u, v$ | flow velocities in $x,\ y$ directions. |
| $v_{fi}$ | settling velocity of the $i$-th class. |
| $z_b$ | topographic elevation of the soil surface. |
| $\alpha$ | parameter used in equation (19). |
| $\beta,\ \kappa$ | parameters used in equation (29). |
| $\gamma^*$ | parameter used in equation (27). |
| $\Delta x, \Delta t$ | space and time steps of the scheme. |
| $\rho_w,\ \rho_s$ | density of water and sediment particle. |
| $\phi$ | porosity of the bed. |
| $\omega,\ \omega_{cr}$ | stream power and its critical value. |

## Acknowledgments

The data for the two-dimensional test case are available at `http://www.umr-lisah.fr/Thies_2004/`.

This work was supported by the ANR VMCS program BIOCRUST. The authors would like to thanks Frédéric Darboux for the numerous discussions, comments and suggestions. We are also grateful to the anonymous referees and to the editor for the numerous improvements suggested.

## References

H. Aksoy, and M. L. Kavvas (2005), A review of hillslope and watershed scale erosion and sediment transport models, *CATENA*, *64*(2-3), 247 – 271, doi:http://dx.doi.org/10.1016/j.catena.2005.08.008,

25 Years of Assessment of Erosion.

E. Audusse, and M.-O. Bristeau (2003), Transport of pollutant in shallow water: A two time steps kinetic method, *M2AN*, *37*(2), 389–416, doi:10.1051/m2an:2003034.

E. Audusse, and M.-O. Bristeau (2005), A well-balanced positivity preserving "second-order" scheme for shallow water flows on unstructured meshes, *Journal of Computational Physics*, *206*, 311–333, doi:10.1016/j.jcp.2004.12.016.

E. Audusse, F. Bouchut, M.-O. Bristeau, R. Klein, and B. Perthame (2004), A fast and stable well-balanced scheme with hydrostatic reconstruction for shallow water flows, *SIAM J. Sci. Comput.*, *25*(6), 2050–2065, doi:10.1137/S1064827503431090.

D. Barry, G. Sander, S. Jomaa, B. Heng, J.-Y. Parlange, I. Lisle, and W. Hogarth (2010), Exact solutions of the Hairsine–Rose precipitation-driven erosion model for a uniform grain-sized soil, *Journal of Hydrology*, *389*(3-4), 399–405, doi:10.1016/j.jhydrol.2010.06.016.

P. Batten, N. Clarke, C. Lambert, and D. M. Causon (1997), On the choice of wavespeeds for the HLLC Riemann solver, *SIAM J. Sci. Comput.*, *18*(6), 1553–1570, doi:10.1137/S1064827593260140.

C. Berthon, and F. Foucher (2012), Efficient well-balanced hydrostatic upwind schemes for shallow-water equations, *Journal of Computational Physics*, *231*(15), 4993–5015, doi:10.1016/j.jcp.2012.02.031.

L. Beuselinck, G. Govers, A. Steegen, and T. A. Quine (1999), Sediment transport by overland flow over an area of net deposition, *Hydrological Processes*, *13*(17), 2769–2782.

F. Bouchut (2004), *Nonlinear stability of finite volume methods for hyperbolic conservation laws, and well-balanced schemes for sources*, vol. 2/2004, Birkhäuser Basel, doi:10.1007/b95203.

F. Bouchut, and T. de Luna (2010), A subsonic-well-balanced reconstruction scheme for shallow water flows, *SIAM Journal on Numerical Analysis*, *48*(5), 1733–1758, doi:10.1137/090758416.

M.-O. Bristeau, and B. Coussin (2001), Boundary conditions for the shallow water equations solved by kinetic schemes, *Tech. Rep. 4282*, INRIA.

Z. Cao, R. Day, and S. Egashira (2002), Coupled and decoupled numerical modeling of flow and morphological evolution in alluvial rivers, *Journal of Hydraulic Engineering*, *128*(3), 306–321, doi:10.1061/(ASCE)0733-9429(2002)128:3(306).

Z. Cao, P. Carling, G. Pender, and S. Wallis (2004), Computational dam-break hydraulics over erodible sediment bed, *Journal of Hydraulic Engineering*, *130*, 689–703.

M. Castro, J. Gallardo, and C. Parés (2006), High order finite volume schemes based on reconstruction of states for solving hyperbolic systems with nonconservative products. Applications to shallow-water systems, *Math. Comp.*, *75*(255), 1103–1134.

O. Cerdan, G. Govers, Y. Le Bissonnais, K. Van Oost, J. Poesen, N. Saby, A. Gobin, A. Vacca, J. Quinton, K. Auerswald, A. Klik, F. Kwaad, D. Raclot, I. Ionita, J. Rejman, S. Rousseva, T. Muxart, M. Roxo, and T. Dostal (2010), The rate and spatial distribution of soil erosion in Europe: A study based on erosion plot data, *Geomorphology*, *122*, 167–177, doi:10.1016/j.geomorph.2010.06.011.

N. Cheng(1997), Simplified settling velocity formula for sediment particle, *J. Hydraul. Eng*, *123*(2), 149–152.

O. Delestre, S. Cordier, F. Darboux, and F. James (2012), A limitation of the hydrostatic reconstruction technique for shallow water equations, *Comptes Rendus Mathematique*, *350*(13–14), 677–681, doi: 10.1016/j.crma.2012.08.004.

O. Delestre, C. Lucas, P.-A. Ksinant, F. Darboux, C. Laguerre, T.-N.-T. Vo, F. James, and S. Cordier (2013), SWASHES: a compilation of Shallow Water Analytic solutions for Hydraulic and Environmental Studies, *International Journal for Numerical Methods in Fluids*, *72*(3), 269–300, doi: 10.1002/fld.3741.

O. Delestre, F. Darboux, F. James, C. Lucas, C. Laguerre, and S. Cordier (2014), FullSWOF: A free software package for the simulation of shallow water flows, submitted (`https://hal.archives-ouvertes.fr/hal-00932234v1`).

A. Duran, Q. Liang, and F. Marche (2013), On the well-balanced numerical discretization of shallow water equations on unstructured meshes, *Journal of Computational Physics*, *235*(0), 565 – 586, doi:http://dx.doi.org/10.1016/j.jcp.2012.10.033.

A. Farenhorst, and R. Bryan (1995), Particle size distribution of sediment transported by shallow flow, *CATENA*, *25*(1–4), 47 – 62, doi:10.1016/0341-8162(94)00041-C.

P. Fiener, G. Govers, and K. V. Oost (2008), Evaluation of a dynamic multi-class sediment transport model in a catchment under soil-conservation agriculture, *Earth Surface Processes and Landforms*, *33*(11), 1639–1660, doi:10.1002/esp.1634.

T. Gallouët, J.-M. Hérard, and N. Seguin (2003), Some approximate godunov schemes to compute shallow-water equations with topography, *Computers & Fluids*, *32*, 479–513.

G. Govers, J. Poesen, A. Knapen, G. Gyssels, and J. Nachtergaele (2007), Resistance of soils to concentrated flow erosion: A review, *Earth-Science Reviews*, *80*, 75–109.

W. Green, and G. Ampt (1911), Studies on soil physics, *The Journal of Agricultural Science*, *4*, 1–24.

J. M. Greenberg, and A.-Y. LeRoux (1996), A well-balanced scheme for the numerical processing of source terms in hyperbolic equation, *SIAM Journal on Numerical Analysis*, *33*, 1–16.

P. Hairsine, and C. Rose (1991), Rainfall detachment and deposition: Sediment transport in the absence of flow-driven processes, *Soil Sci. Soc. Am. J.*, *55*(2), 320–324.

P. Hairsine, and C. Rose (1992), Modeling water erosion due to overland flow using physical principles. II: rill flow, *Water Resources Research*, *28*, 245–250.

P. Hairsine, L. Beuselinck, and G. Sander (2002), Sediment transport through an area of net deposition, *Water Resources Research*, *38*(6), 22–1–22–7, doi:10.1029/2001WR000265.

A. Harten, P. Lax, and B. van Leer (1983), On upstream differencing and Godunov-type schemes for hyperbolic conservation laws, *SIAM Review*, *25*(1), 35–61.

B. Heng, G. Sander, and C. Scott (2009), Modeling overland flow and soil erosion on nonuniform hillslopes: A finite volume scheme, *Water Resources Research*, *45*(5), W05,423, doi:10.1029/2008WR007502.

B. Heng, G. Sander, A. Armstrong, J. Quinton, J. Chandler, and C. Scott (2011), Modeling the dynamics of soil erosion and size-selective sediment transport over nonuniform topography in flume-scale experiments, *Water Resour. Res.*, *47*(2), W02,513.

J.-M. Hervouet (2007), *Hydrodynamics of Free Surface Flows: Modelling with the Finite Element Method*.

W. Hogarth, J.-Y. Parlange, C. Rose, G. Sander, T. Steenhuis, and A. Barry (2004), Soil erosion due to rainfall impact with inflow: an analytical solution with spatial and temporal effects, *Journal of Hydrology*, *295*(1-4), 140–148, doi:10.1016/j.jhydrol.2004.03.007.

J. Hou, Q. Liang, F. Simons, and R. Hinkelmann (2013), A 2d well-balanced shallow flow model for unstructured grids with novel slope source term treatment, *Advances in Water Resources*, *52*(0), 107 – 131, doi:http://dx.doi.org/10.1016/j.advwatres.2012.08.003.

J. Kim, and V. Y. Ivanov (2014), On the nonuniqueness of sediment yield at the catchment scale: The effects of soil antecedent conditions and surface shield, *Water Resources Research*, *50*(2), 1025–1045, doi:10.1002/2013WR014580.

J. Kim, V. Y. Ivanov, and N. D. Katopodes (2013), Modeling erosion and sedimentation coupled with hydrological and overland flow processes at the watershed scale, *Water Resources Research*, *49*(9), 5134–5154, doi:10.1002/wrcr.20373.

R. LeVeque (2002), *Finite volume methods for hyperbolic problems*, Cambridge Texts in Applied Mathematics, xx+558 pp., Cambridge University Press, Cambridge.

S. Li, and C. J. Duffy (2011), Fully coupled approach to modeling shallow water flow, sediment transport, and bed evolution in rivers, *Water Resources Research*, *47*(3), n/a–n/a, doi: 10.1029/2010WR009751.

Q. Liang, and F. Marche (2009), Numerical resolution of well-balanced shallow water equations with complex source terms, *Advances in Water Resources*, *32*(6), 873–884, doi:10.1016/j.advwatres.2009.02.010.

R. I. McLachlan, and G. R. W. Quispel (2002), Splitting methods, *Acta Numerica*, *11*, 341–434, doi: 10.1017/S0962492902000053.

W. Merritt, R. Letcher, and A. Jakeman (2003), A review of erosion and sediment transport models, *Environm. Model. Software*, *18*(8-9), 761–799.

C. Mügler, O. Planchon, J. Patin, S. Weill, N. Silvera, P. Richard, and E. Mouche (2011), Comparison of roughness models to simulate overland flow and tracer transport experiments under simulated rainfall at plot scale, *Journal of Hydrology*, *402*(1-2), 25 – 40, doi:http://dx.doi.org/10.1016/j.jhydrol.2011.02.032.

J. Murillo, P. GarcÃa-Navarro, P. Brufau, and J. Burguete (2008), 2d modelling of erosion/deposition processes with suspended load using, *Journal of Hydraulic Research*, *46*(1), 99–112, doi:10.1080/00221686.2008.9521847.

G. Nord, and M. Esteves (2005), Psem-2d: A physically based model of erosion processes at the plot scale, *Water Resources Research*, *41*, 08,407.

A. Proffitt, C. Rose, and P. Hairsine (1991), Rainfall detachment and deposition: experiments with low slopes and significant water depths, *Soil Sci. Soc. Am. J.*, *29*, 671–683.

J. Quinton, G. Govers, K. Van Oost, and R. Bardgett (2010), The impact of agricultural soil erosion on biogeochemical cycling, *Nature Geoscience*, *3*, 311–314, doi:10.1038/ngeo838.

C. Rose, B. Yu, H. Ghadiri, H. Asadi, J. Parlange, W. Hogarth, and J. Hussein (2007), Dynamic erosion of soil in steady sheet flow, *Journal of Hydrology*, *333*, 449–458.

G. Sander, P. Hairsine, C. Rose, D. Cassidy, J.-Y. Parlange, W. Hogarth, and I. Lisle (1996), Unsteady soil erosion model, analytical solutions and comparison with experimental results, *Journal of Hydrology*, *178*(1–4), 351–367, doi:10.1016/0022-1694(95)02810-2.

G. Sander, P. Hairsine, L. Beuselinck, and G. Govers (2002), Steady state sediment transport through an area of net deposition: Multisize class solutions, *Water Resources Research*, *38*(6), 23–1–23–8, doi:10.1029/2001WR000323.

G. Sander, J.-Y. Parlange, D. A. Barry, M. B. Parlange, and W. L. Hogarth (2007), Limitation of the transport capacity approach in sediment transport modeling, *Water Resources Research*, *43*(2), doi:10.1029/2006WR005177.

G. Simpson, and S. Castelltort (2006), Coupled model of surface water flow, sediment transport and morphological evolution, *Computers and Geosciences*, *32*, 1600–1614.

J. J. Stoker, (1957), *Water Waves: The Mathematical Theory with Applications*, Interscience Publishers, New York, USA.

L. Tatard, O. Planchon, J. Wainwright, G. Nord, D. Favis-Mortlock, N. Silvera, O. Ribolzi, M. Esteves, and C.-h. Huang (2008), Measurement and modelling of high-resolution flow-velocity data under simulated rainfall on a low-slope sandy soil, *Journal of Hydrology*, *348*(1-2), 1–12, doi:10.1016/j.jhydrol.2007.07.016.

E. Toro (2001), *Shock-Capturing Methods for Free-Surface Shallow Flows*, Wiley and Sons Ltd.

B. van Leer (1979), Towards the ultimate conservative difference scheme. V. A second-order sequel to Godunov's method, *Journal of Computational Physics*, *32*(1), 101–136, doi:DOI:10.1016/0021-9991(79)90145-1.

K. Van Oost, L. Beuselinck, P. B. Hairsine, and G. Govers (2004), Spatial evaluation of a multi-class sediment transport and deposition model, *Earth Surface Processes and Landforms*, *29*(8), 1027–1044, doi:10.1002/esp.1089.

D. Woolhiser, and J. Liggett (1967), Unsteady, one-dimensional flow over a plane–the rising hydrograph, *Water Resources Research*, *3*(3), 753–771.